Mechatronics and Automation Technology
J.-Y. Xu (Ed.)

doi:10.3233/ATDE231109

Machining-Oriented Contact Analysis Based on the Modeling of the RV Cycloid Planetary Reducer

Lei YANG, Yu LUO[1], Yanlei LUO, Wei DU, Xiang ZHENG and Ya LI

School of Mechanical Engineering, Guizhou University, Guiyang 550025, Guizhou, China

Abstract. A RV cycloid planetary reducer used in the excavator chassis is studied. A contact model based on impulse function is proposed to define the constraint between the contact parts during the working condition. The contact parameters in the contact model includes: Contact stiffness, index of force, damped coefficient and depth of penetration. Among them the unique undetermined one is contact stiffness, which is studied under two working conditions. These conditions are Convex-Convex Contact (pin-top of cycloid) and Convex-Concave Contact (pin-dedendum of cycloid). Analysis of the contact parameters indicates that the contact stiffness is affected by the contact thickness. The performance of the reducer part material must satisfy these parameters. Then a dynamic model of the RV cycloid planetary reducer is built, in which the contact force model is utilized to realize the constraint of pin-cycloid wheel, planetary wheel-sun wheel. The simulate results of idle load and full load indicate that the deviation of output draft angular velocity between simulation and theoretical is 0.83%. The work envelope of the center of the cycloid mass is a circle, and the circle radius is eccentric distance of the two cycloids. The simulation of contact moment between the pins and cycloid reveals only six contacts exist at any instant, and the maximum moment appears at the middle contact pair. This contact constraint model can be used to direct the machining of the wheels and the process of reducer assembly.

Keywords. RV cycloid planetary reducer; Contact constraint model; Impulse function; Machining-oriented; Material selection.

1. Introduction

The cycloid planetary reducer is widely used in space craft, modern robot and construction machinery. In order to improve the transmission efficiency, life and smoothness of operation, the studies focus on the aspects of manufacturing processes [1,2], force analysis [3-5], meshing characteristics [6,7], novel structure [8,9] and parts optimization [10-12]. Most of these researches need a virtual model to verify the theoretical analysis, which can save the cost of experiments.

This study gives a regime to model a virtual cycloid planetary reducer used on the chassis of excavator mainly. The impulse function is used to build a contact model to depict the constraint of cycloid and pins, in which the relation of contact stiffness to

[1] Corresponding Author, Yu LUO, School of Mechanical Engineering, Guizhou University, Guiyang 550025, China; E-mail: 18786304214@163.com.

contact thickness is deduced. A comparison of the reducer transmission ratio between the theoretical and simulation results reveals that the dynamic model reflects the operation process of the reducer accurately. The model can also reflect the contact moment between pins and cycloid. The simulation of contact moment between the pins and cycloid is as the external force applied to the subsequent analysis to estimate stress and strain, natural frequency etc. The method and model in this paper can be used for testing and analysis, thus save physical experimental cost.

2. Dynamic Model of Cycloid Planetary Reducer

2.1. Structure of Cycloid Planetary Reducer

The RV cycloid planetary reducer caters to the chassis of the excavator. It is composed of two stages. The first stage is a traditional involute planetary transmission. The second stage is a pin-cycloid planetary transmission. The transmission diagram of this planetary transmission mechanism is shown in figure 1, and figure 2 is the main view of assembly. Z1 is the sun gear of first stage, which is made as a gear shaft. The input shaft is connected to walking hydraulic motor. Three planet gears Z2 are circular distribution. Crank 5 is assembled with Z2, which connects the two transmission stages. Z4 are pins fixed in the static pin gear housing. Component Z3 consists of two cycloids. There is an eccentric distance (a = 4.5 mm) between the two centers of the cycloids. The Assembly requirements is gear tooth top of the front cycloid aligning to tooth root of the rear cycloid. The output shaft is bolted to the planet shelf called W-mechanism. W-mechanism drives the driving wheel of the chassis.

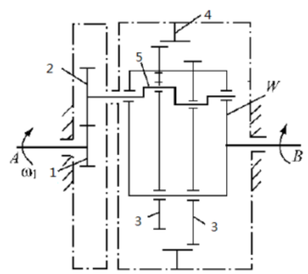

Figure 1. Transmission diagram of RV planetary transmission mechanism.

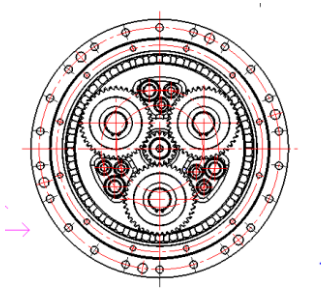

Figure 2. Assembly main view of planetary transmission mechanism.

2.2. Principle of Operation

Gear shaft Z1 is assembled to the output shaft of hydraulic motor, which provides the input power. Z1 transmits power to Z2 through meshing. Z2 turns the crank 5 to rotate. A bearing lying on crank 5 supports cycloids Z3, makes cycloids Z3 rotating around the center axis of the reducer. On the other hand, the meshing between cycloids Z3 and pins Z4 leads to the revolution of cycloids on their own axes. The output shaft B is driven by cycloids Z3 through contact force.

The transmission ratio i is the product of the transmission ratio of the two stages. The first stage is the involutes planetary gears, and the transmission ratio is

$$i_{12}^{w} = -\frac{z_2}{z_1} = \frac{n_1 - n_w}{n_2 - n_w} \tag{1}$$

The second stage is the cycloid planetary gears, and the transmission ratio is

$$i_{34}^{5} = \frac{z_4}{z_3} = \frac{n_3 - n_5}{n_4 - n_5} \tag{2}$$

The pins Z4 are fixed, $n_4 = 0$. The crank 5 and planetary gears Z2 are assembled together, so $n_5 = n_2$. As the action of contact force, the rotation of cycloid gears Z3 is transferred to output shaft, so $n_3 = n_w$. Then equation (2) can be

$$\frac{z_4}{z_3} = 1 - \frac{n_w}{n_2} \tag{3}$$

According to Eq.1 and Eq.3, the transmission ratio i is

$$i = \frac{n_{in}}{n_{out}} = 1 + \frac{z_2}{z_1} \times z_4 \tag{4}$$

If the parameters are substituted by the number of sun wheel teeth 18, the planet wheel teeth 42 on the first stage, the number of pin teeth 24 on second stage. The calculation of transmission ratio is$i = 57$.

3. Contact Force External to Cycloid Planetary Reducer

3.1. Contact Force

The contact force is adopted to define the constraint relation of pins and cycloids during modeling rather than joint [13], because there is no joint exist between them. Two methods can be used to depict the contact force, (1) compensation and (2) impulse function [14]. The latter is chosen to study the RV cycloid planetary reducer in which four key parameters considered are contact stiffness $\boldsymbol{k}$, force index $\boldsymbol{e}$, damped coefficient$\boldsymbol{d}$ and depth of penetration$\boldsymbol{x}$. The maximum of damp depends on the depth of penetration. According to the empirical value and reference [15], $\boldsymbol{e = 1.5}$, $\boldsymbol{x = 0.01\ mm}$,$\boldsymbol{d = 1 \times 10^2\ N/SEC \times mm}$.

The unique undetermined parameter is contact stiffness$k$. The harder the materials of contact bodies are, the higher the contact stiffness of parts is. The unit of contact stiffness$k$ is N/mm. the derivation of $k$is shown below.

$$k = k' \times \sqrt{w} \tag{5}$$

where k' is stiffness coefficient,

$$k' = \frac{4}{3} E \cdot \sqrt{R} \tag{6}$$

where

$$R = \frac{R_1 \cdot R_2}{R_1 + R_2} \tag{7}$$

R_1 is the pitch radius of pin (mm)， R_2 is the pitch radius of cycloid(mm). Derivation of E is shown in Eq.8.

$$E = \frac{1-\mu_1^2}{E_1} - \frac{1-\mu_2^2}{E_2} \tag{8}$$

Where E_1,E_2 is the elastic modulus of material， $E_1 = E_2 = 2.17 \times 10^5 \mathrm{N/mm^2}$, μ_1,μ_2 is poisson's ratio of material， $\mu_1 = \mu_2 = 0.3$.

According to Hertz, if the contact thickness of pin and cycloid is$L$, the contact deformation w is,

$$w = \frac{2F}{\pi L}\left[\frac{1-\mu_1^2}{E_1}\left(\frac{1}{3} + ln\frac{4R_1}{b}\right) + \frac{1-\mu_2^2}{E_2}\left(\frac{1}{3} + ln\frac{4R_2}{b}\right)\right] \tag{9}$$

where$F$is pressure force between pin and cycloid, and the unit is [N]，

$$F = k' \cdot x^e \tag{10}$$

$$b = 1.60\sqrt{\frac{F}{L} \cdot k_D \cdot \left(\frac{1-\mu_1^2}{E_1} - \frac{1-\mu_2^2}{E_2}\right)} \tag{11}$$

If the contact between pins and cycloids is at the top of the tooth, the equivalent curvature radius (ECR) is $k_D = \frac{2R_1R_2}{R_1+R_2}$. If the contact occurring at the dedendum of cycloid, the ECR is $k_D = \frac{2R_1R_2}{R_2-R_1}$.

3.2. Analysis of Contact Stiffness

Once the material of pins and cycloids is determined, the elastic modulus, poisson's ratio, force index and depth of penetration are constant. Once the geometric dimension of pins and cycloids is set, the $\boldsymbol{R}$ in equation (7) is constant. The equations (8)-(11) indicates the trends of contact stiffness $\boldsymbol{k}$ following the changing trend of contact width $\boldsymbol{L}$. If the pitch radius of pin and cycloid are introduced in the equation (7), along with the change of contact width, the corresponding contact stiffness coefficient is shown in figure 3.

Two work condition, (1) contact between pin and cycloid at the top of the tooth (Convex-Convex Contact), (2) contact occurring at the dedendum of cycloids (Convex-Concave Contact). The curve trend of contact stiffness with the contact thickness is consistent in two situations. The maximum appear at the point that contact width is about 5mm. The maximum of condition (1) is$3.988 \times 10^5 N/mm^2$, whereas the condition (2) is $5.093 \times 10^5 \mathrm{N/mm^2}$.

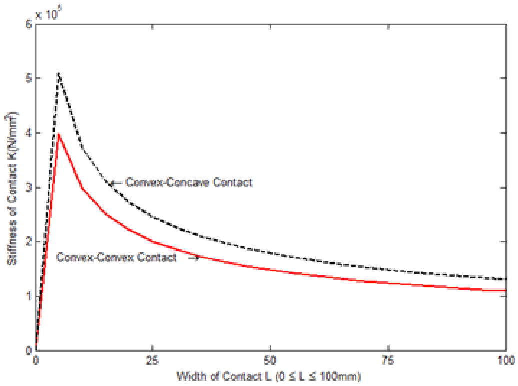

Figure 3. The relationship between Contact width and Contact stiffness.

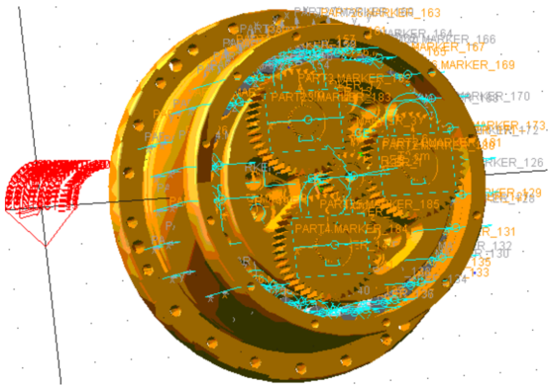

Figure 4. Dynamic Model of RV Cycloid Planetary Reducer.

3.3. Exerting Contact Force

The contact relation between pins and cycloids are contact force collision of the bodies [16]. The corresponding parameters can be computed through Equations (5)-(11). Considering the material of planetary wheels is inferior to the cycloids, the same parameters can be used in the contact of planetary wheels and sun wheel. The simulation system searches 51 contacts automatically. The figure 4 is the dynamic model with the contact parameters.

4. Simulation of Cycloid Planetary Reducer

4.1. Setting up Driving Parameter

This RV cycloid planetary reducer is suitable for small to medium type excavator chassis. The power is 112 kw, travel velocity is from 3.3 km/h to 5.5 km/h, minimum ground clearance is 0.44 m.

Take 3.3 km/h as an example. The angular velocity of output shaft is computed by $\omega = \frac{v}{r}$. The angular velocity of input shaft is obtained by ω multiplying the transmission ratio 57, and value is 8328 deg/s. According to the power formula, the input torque is calculated as $M_B = 4024.9$ Nm. Assuming no loss power of the excavator engine exist in working, then $n_A \cdot M_A = n_B \cdot M_B$ is workable, then $M_A = 770.6$ Nm.

4.2. Simulation based on Dynamic Model

In the idle load work condition, the motion excitation is input angular velocity acting on the sun wheel, and the value is 8328deg/s. The theoretical output angular velocity is 146.1deg/s, in contrast to the simulation angular velocity 144.9deg/s, The simulation curve is shown in figure 5.

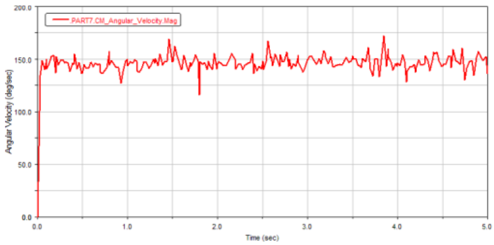

Figure 5. Real-time simulation curve of output shaft angular velocity under idle load.

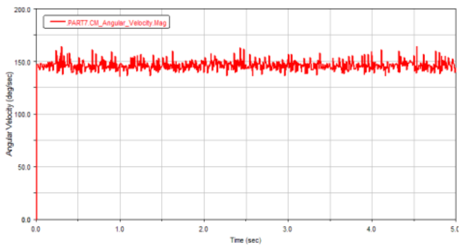

Figure 6. Real-time Simulation curve of output shaft angular velocity under full load.

When the input angular velocity is 8328 deg/s, a great impact can be seen at the moment of starting the simulation. It is because of the sudden infliction of the input motion. Then the angular velocity fluctuates around an average value, which is 144.9 deg/s. the deviation between theoretical and simulated value is 0.83%. It means the transmission ratio of dynamic model is fluctuates around the theoretical value under idle load. The reason leads to swing of input angular velocity is probably the clearance between parts, and inertial force of parts during working.

If load is considered, the torque can be set on the output shaft as the value is 4024.9 Nm, and the input shaft as the value is 770.6 Nm. The motion excitation is 8328 deg/s.

The simulation curve is shown in figure 6.

Figure 6 shows that the trend of output shaft angular velocity is same to idle load condition. But the vibration frequency is bigger than that of idle load condition, whereas the amplitude is smaller than that of idle load condition. After the great impact in minute time, the output shaft angular velocity fluctuates around an average value, which is 144.9deg/s. The transmission ratio of dynamic model is fluctuates around the theoretical value under full load, which can guarantee the transmission.

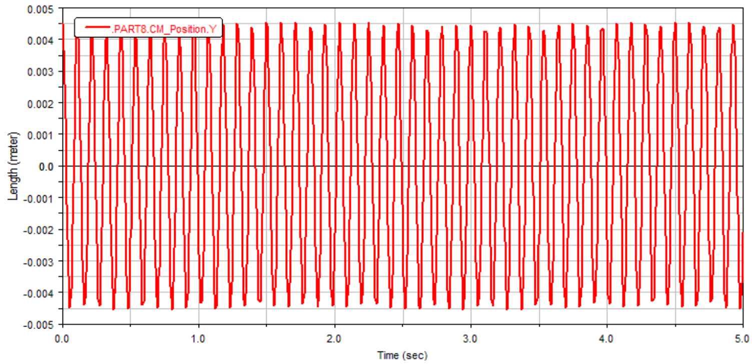

Figure 7. Center of mass displacement of front cycloid

Figure 7 is the center of mass displacement of front cycloid. The distance between center of front cycloid mass and axis y fluctuates at the interval from -0.0045 m to 0.0045 m. This interval is as twice as the eccentric distance (a = 4.5 mm). The center of rear cycloid mass displacement is similar to figure 7, but there is a delay in time, because the angular deviation between the front and rear cycloid.

5. Analysis of Contact Moment between Cycloid and Pins

The contact constraint can be verified through the dynamic model by the factor of contact moment [17]. To avoid the mistakes arisen by unstable factors during operation [18,19] at initial phase, such as impact load [20]. Take the front cycloid as an example, the virtual dynamic model simulate the contact moment around 4.92s, which is about two cycle time.

Facilitating description, the 24 pins on the cycloid planetary reducer are numbered. Pair i means the contact moment between pins i and cycloid. It is impossible that the front cycloid contact with all pins at any instant. The study focuses on not only the time – contact moment at one pin, but also the moment variation about the adjacent pins. The contact moment between a set of pins and cycloid is shown in figures 8-14.

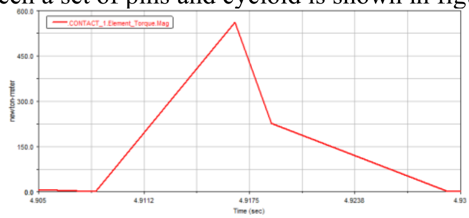

Figure 8. contact moment between pin2-front cycloid.

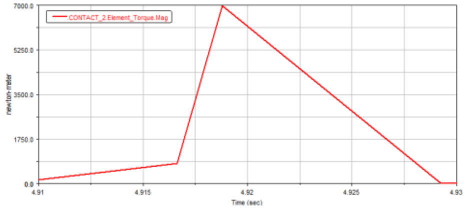

Figure 9. contact moment between pin1-front cycloid.

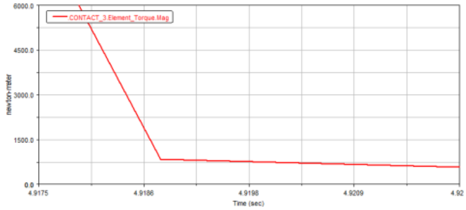

Figure 10. contact moment between pin3-front cycloid.

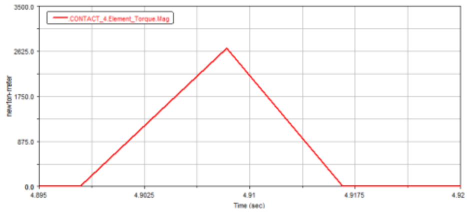

Figure 11. contact moment between pin4 and front cycloid.

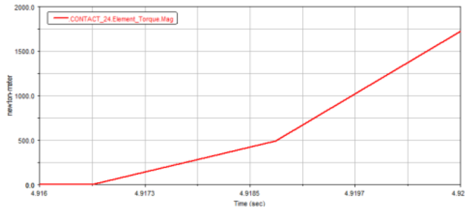

Figure 12. contact moment between pin24-front cycloid.

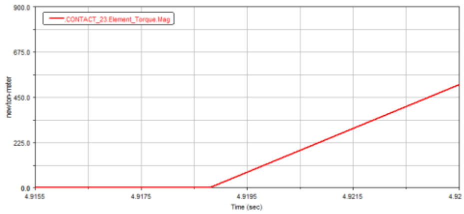

Figure 13. contact moment between pin23-front cycloid (pin 24 adjacent to pin1).

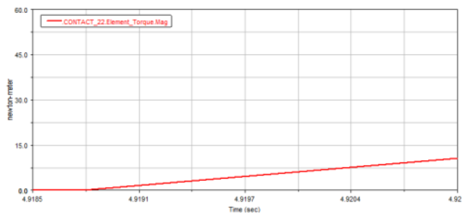

Figure 14. contact moment between pin22-front cycloid

At 4.92 s, the maximum value of contact moment appears at the pair 24 in figure 12. In figures 12-14, the contact moment increases gradually from pair 22 to pair 24. On the other hand, the contact moment decreases gradually from pair 1 to pair4. The contact moments of pair1 and pair 23 are approximate. Pair 4 is zero means no contact. So, there are six pins contacting with the front cycloid at any instant.

It is noticed that contact moments at pair 2 and pair 3 in figures 9 and 10 are abnormal large. This may be caused by the huge inertial moment during the rotation of cycloids, or by the ill-conditioned problem of equation, even the combination of two reasons.

The analysis results of contact moment are useful in following analysis or optimization. For example, the data is as the external force applied to the FEA model for static analysis.

6. Conclusion

The RV cycloid planetary reducer studying is composed of two stages. The transmission ratio depends on the teeth numbers of sun wheel of the first stage, the planet wheel of the first stage and the pin wheel of the second stage. Expect the joint constraint, the contact constraint of pin and cycloid, sun and planet have to be considered during the dynamic modeling. The contact constraint can be depicted through the impulse function of contact model. The parameters include force index e, damped coefficient d and depth of penetration x, which can be estimated by empirical value. The contact stiffness k in contact model depends on the structure and geometric parameters. The research gives the relation of contact width and contact stiffness.

The parameters of contact model are set on the dynamic model. Simulation has done on the dynamic model under idle load and full load work conditions. In idle load condition, only motion excitation is used to drive the reducer, the results indicate the deviation between theoretical and simulated value is 0.83%. In full load condition, except motion excitation, input and output torque are also needed to drive. The results indicate that the vibration frequency of output shaft angular velocity is bigger and the amplitude is smaller than that of idle load.

The contact constraint can be verified by the analysis of contact moment based on the virtual dynamic model. In one rotate cycle of cycloid, not all the teeth of cycloid mesh with the pins. Six meshing pins are found at any instant during simulation. The maximum contact moment appears at the middle meshing pair between cycloid teeth and pin. And the moment gradually reduces to both side pairs, until no contact exists.

The contact model and analysis result are used not only in building dynamic model, but also in subsequent analysis and optimization. The static analysis in FEA, for example, the contact model is used as constraint, and the contact moment is as external force to estimate the stress- strain.

Acknowledgements

This Research is funded by the Basic Research Project of Guizhou ZK [2022] general 087, the State Scholarship Fund of China [201906675018], National Science Foundation of China [52265007].

References

[1] Dai H, Chen F and Xun C, et al. Numerical calculation and experimental measurement for gear mesh force of planetary gear transmissions[J]. Mechanical Systems and Signal Processing, 2022, 162: 108085.
[2] Chen Z, Zhou Z and Zhai W, et al. Improved analytical calculation model of spur gear mesh excitations with tooth profile deviations[J]. Mechanism and Machine Theory, 2020, 149: 103838.
[3] Wang H, Shi Z -Y and Yu B, et al. Transmission Performance Analysis of RV Reducers Influenced by Profile Modification and Load[J]. Applied Sciences, 2019, 9: 4099.
[4] Li G, Wang Z and Kubo A. Error-sensitivity analysis for hypoid gears using a real tooth surface contact model[J]. Proceedings of the Institution of Mechanical Engineers, Part C: Journal of Mechanical Engineering Science, 2017, 231: 507–521.
[5] Kumar N, Kosse V and Oloyede A. A new method to estimate effective elastic torsional compliance of single-stage Cycloidal drives[J]. Mechanism and Machine Theory, 2016, 105: 185–198.
[6] David B. Dooner. On the third law of gearing: A study on hypoid gear tooth contact[J]. Mechanism and Machine Theory, 2019, 134: 224–248.
[7] Song Y, Liao Q and Wei S, et al. Modelling, simulation and experiment of a novel pure rolling cycloid reducer with involute teeth[J]. IJMIC, 2014, 21: 184.
[8] Dawei Li, Yongping Liu and Jun Gong, et al. Design of a Noncircular Planetary Gear Mechanism for Hydraulic Motor[J]. Mathematical Problems in Engineering, 2021, 2021: 1–9.
[9] Duan H, Li L and Tao J. Structure design and motion simulation of the pin-cycloid gear planetary reducer with ring-plate-type[J]. IOP Conf. Ser.: Earth Environ. Sci., 2017, 69: 012183.
[10] Huang J, Li C and Zhang Y, et al. Transmission error analysis of cycloidal pinwheel meshing pair based on rolling–sliding contact[J]. J. Braz. Soc. Mech. Sci. Eng., 2021, 43: 355.
[11] Zhang T, Li X and Wang Y, et al. A Semi-Analytical Load Distribution Model for Cycloid Drives with Tooth Profile and Longitudinal Modifications[J]. Applied Sciences, 2020, 10: 4859.
[12] Wang J, Luo S and Su D. Multi-objective optimal design of cycloid speed reducer based on genetic algorithm[J]. Mechanism and Machine Theory ,2016, 102: 135–148.
[13] Chen X, Jiang S and Deng Y, et al. Dynamics analysis of 2-DOF complex planar mechanical system with joint clearance and flexible links[J]. Nonlinear Dyn., 2018, 93: 1009–1034.
[14] ADAMS entry detailed explanation and examples. Beijing[M]: Tsinghua University Press, 2021.
[15] Chen X, Jiang S and Deng Y, et al. Dynamics analysis of 2-DOF complex planar mechanical system with joint clearance and flexible links[J]. Nonlinear Dyn., 2018, 93: 1009–1034.
[16] Liu J, Wang L and Ma J, et al. A multi-body dynamic study of vibration of a planetary gear train with the planetary bearing fault[J]. Proceedings of the IMechE, 2019, 233: 677–695.
[17] Fortais A, Loukiantchenko E and Dalnoki-Veress K. Writhing and hockling instabilities in twisted elastic fibers[J]. Eur. Phys. J E, 2021, 44: 149.
[18] Meng Z, Shi G and Wang F. Vibration response and fault characteristics analysis of gear based on time-varying mesh stiffness[J]. Mechanism and Machine Theory 2020, 148: 103786.
[19] Wang R, Gao F and Lu M, et al. Meshing Efficiency Analysis of Modified Cycloidal Gear Used in the RV Reducer[J]. Tribology Transactions, 2019; 62: 337–349.
[20] González F, Kövecses J and Font-Llagunes J M. Load assessment and analysis of impacts in multibody systems[J]. Multibody Syst. Dyn., 2016, 38: 1–19.